NATIONAL ADVISORY COMMITTEE FOR AERONAUTICS

TECHNICAL NOTE 3896

SUBSONIC WIND-TUNNEL INVESTIGATION OF THE EFFECT OF FUSELAGE AFTERBODY ON DIRECTIONAL STABILITY OF WING-FUSELAGE COMBINATIONS AT HIGH ANGLES OF ATTACK

By Edward C. Polhamus and Kenneth P. Spreemann

Langley Aeronautical Laboratory
Langley Field, Va.

Washington
December 1956

M

NATIONAL ADVISORY COMMITTEE FOR AERONAUTICS

TECHNICAL NOTE 3896

SUBSONIC WIND-TUNNEL INVESTIGATION OF THE EFFECT OF FUSELAGE AFTERBODY ON DIRECTIONAL STABILITY OF WING-FUSELAGE COMBINATIONS AT HIGH ANGLES OF ATTACK

By Edward C. Polhamus and Kenneth P. Spreeman

SUMMARY

A wind-tunnel study of the directional stability characteristics at high angles of attack of two wing-fuselage combinations has been conducted at subsonic speeds. The wings utilized were a 4-percent-thick unswept wing of aspect ratio 3.0 and a 6-percent-thick 45° sweptback wing of aspect ratio 4. The results indicated very large differences in the directional stability between the two wing-fuselage configurations at high angles of attack. The unswept-wing—fuselage combination became stable at high angles, whereas the sweptback-wing—fuselage combination became increasingly unstable. Tests with the fuselage afterbody removed indicated that these effects were associated with wing induced sidewash over the fuselage afterbody.

INTRODUCTION

The current trend of aircraft toward high fuselage mass loadings and long nose lengths has created several adverse effects with regard to aircraft motions. For example, this trend has increased the tendency toward the violent oscillatory type of spin (ref. 1); and, as pointed out in reference 2, high fuselage mass loadings may result in dangerous attitudes being reached in rapid rolls. Since extremely high attitudes can be encountered during both of these motions, it is desirable to maintain adequate static directional stability even well beyond the angle of attack for maximum lift. Unfortunately, large deficiencies in static directional stability are very often encountered at high angles of attack and are, to a large extent, traceable to losses in vertical-tail effectiveness due to unfavorable flow fields induced in the region of the tail of the wing-fuselage combination. (See ref. 3.) However, in addition to the loss in tail effectiveness, rather large variations in directional stability with angle of attack can occur for wing-fuselage combinations with

unswept wings usually providing a favorable decrease in the wing-fuselage directional instability at high angles of attack; whereas the opposite (undesirable) trend usually occurs for sweptback wings. (See ref. 3.) Therefore, a better understanding of these wing-fuselage trends would be very desirable as a possible aid in avoiding the undesirable characteristics and further improving the desirable characteristics. Large effects associated with wing sweep occur even relative to the body axis; and inasmuch as little, if any, leading-edge suction is developed at the high angles of attack involved, it would appear that these large effects are not associated with any yawing-moment changes incurred on the wing itself, but most probably are induced by the wing on the fuselage afterbody. The purpose of the present investigation, therefore, is to determine the effect of fuselage-afterbody length on the static directional stability characteristics of several wing-fuselage configurations.

COEFFICIENTS AND SYMBOLS

The axis system used and the direction of positive forces, moments, and angles are presented in figure 1. Except for the lift and drag, the body-axis system is used. The origin of the axis system is located at the projection on the plane of symmetry of the quarter-chord point of the wing mean aerodynamic chord.

A aspect ratio, b^2/S

b wing span, ft

c local wing chord, ft

$\bar{c}$ mean aerodynamic chord, $\frac{2}{S}\int_0^{b/2} c^2 dy$, ft

C_D drag coefficient, $\frac{\text{Drag}}{qS}$

C_L lift coefficient, $\frac{\text{Lift}}{qS}$

C_l rolling-moment coefficient, $\frac{\text{Rolling moment}}{qSb}$

C_m pitching-moment coefficient, $\frac{\text{Pitching moment}}{qS\bar{c}}$

C_n yawing-moment coefficient, $\frac{\text{Yawing moment}}{qSb}$

C_Y lateral-force coefficient, $\frac{\text{Lateral force}}{qS}$

M free-stream Mach number

q dynamic pressure, $\frac{1}{2}\rho V^2$, lb/sq ft

S total wing area, sq ft

V free-stream velocity, ft/sec

X,Y,Z Cartesian coordinates (fig. 1)

y coordinate along Y-axis, measured from plane of symmetry

α angle of attack, deg

β angle of sideslip, deg

λ wing taper ratio, $\frac{\text{Tip chord}}{\text{Root chord}}$

Λ sweepback angle of wing quarter-chord line, deg

ρ mass density of air, slugs/cu ft

$C_{l_\beta} = \frac{\partial C_l}{\partial \beta}$

$C_{n_\beta} = \frac{\partial C_n}{\partial \beta}$

$\Delta C_{n_{\beta(WF-F)}}$ C_{n_β} of wing-fuselage combination minus C_{n_β} of fuselage

$C_{Y_\beta} = \frac{\partial C_Y}{\partial \beta}$

MODELS AND TEST EQUIPMENT

Drawings of the models used in the investigation are presented in figure 2. The wing having an unswept half-chord line had an aspect ratio of 3.0, a taper ratio of 0.50, and NACA 65A004 airfoil sections; and the wing having 45° sweepback of the quarter-chord line had an aspect ratio

of 4.0, a taper ratio of 0.30, and an NACA 65A006 airfoil section parallel to the plane of symmetry. The thin unswept wing was constructed of solid steel and the sweptback wing was constructed of solid aluminum alloy. The same fuselage was used in conjunction with both wings and was of aluminum and steel construction. The ordinates of the fuselage are given in table I. Both wings were placed in a position on the fuselage such that the quarter-chord points of their respective mean aerodynamic chords were located at 57 percent of the basic fuselage length rearward of the fuselage nose. The rearward 24.7 percent (13.5 inches) of the basic fuselage was removable.

The tests were conducted in the Langley high-speed 7- by 10-foot tunnel, and the models were mounted on the sting-support system shown in figure 3. With this system the angle of attack can be remotely operated and lateral-parameter tests can be obtained (through the angle-of-attack range) by inserting $\pm 4^{\circ}$ couplings in the sting-support system. The aerodynamic forces and moments imposed on the model were determined by means of an internally mounted six-component strain-gage balance.

TESTS AND CORRECTIONS

The tests were conducted at Mach numbers of 0.60 and 0.80 with corresponding Reynolds numbers of 3.0×10^6 and 3.5×10^6, respectively, for the unswept wing and 2.8×10^6 and 3.2×10^6 for the sweptback wing, based on their mean aerodynamic chords.

Blockage corrections as determined by the method of reference 4 have been applied to the Mach number and dynamic pressure. The jet-boundary corrections which were applied to the angle of attack and drag were calculated by the method of reference 5. Only unswept wings were considered in reference 5; however, reference 6 indicates that for the model size utilized in the present investigation the effect of sweep on the jet-boundary corrections is negligible.

No sting tares have been determined for these particular models; however, sting-tare investigations on similar configurations have indicated that the tares should be negligible for the present tailless configurations. The angles of attack and sideslip have been corrected for the deflection of the sting-support and strain-gage balance under load.

RESULTS AND DISCUSSION

Static Longitudinal Characteristics

The static longitudinal characteristics are presented in figures 4, 5, and 6. Inasmuch as there was a program change early in the testing, longitudinal data were not obtained for the unswept wing in combination with the long fuselage at a Mach number of 0.60. Because of the differences in the lengths of the mean aerodynamic chords (fig. 2) used in the coefficients, it was necessary to present the fuselage-alone pitching-moment data in conjunction with both the swept and unswept wings. Since the reference areas are identical, the lift and drag data were repeated only for consistency and convenience.

In general, removal of the fuselage afterbody had little effect on the longitudinal characteristics except for the unswept-wing configuration above an angle of attack of about 10°. Above this angle of attack, removal of the fuselage afterbody resulted in a reduction in lift for the unswept wing-fuselage (fig. 4) which, while small, was considerably greater than the reduction observed for the fuselage-alone configurations. This loss of lift is accompanied with a reduction in the negative pitching moment (fig. 5) and shows that the loss of lift probably occurred on the fuselage afterbody and was not associated to any great extent with possible changes in fuselage induced upwash in the region of the wing. It should be pointed out that, although data with the basic fuselage were not obtained at $M = 0.60$, tests made with a smaller scale model produced results similar to those obtained at $M = 0.80$. The results indicate only minor effects of fuselage afterbody for the sweptback-wing—fuselage configuration. Only minor effects of fuselage afterbody occurred with regard to drag coefficient. (See fig. 6.)

Static Lateral Characteristics

The basic data for static lateral stability, referred to the body axes, are presented in figures 7 to 9. A comparison of the static-lateral-stability derivatives as a function of angle of attack for the unswept- and sweptback-wing—fuselage configurations is presented in figure 7 for Mach numbers of 0.60 and 0.80.

It will be noted that rather large differences exist in the curves for C_{n_β} and C_{l_β} of the sweptback- and unswept-wing configurations. However, inasmuch as the effect of sweep on the effective-dihedral parameter C_{l_β} is fairly well known and is basically a wing-alone phenomenon, the discussion herein is concerned mainly with the directional-stability parameter C_{n_β}.

The results pertaining to C_{n_β} indicate substantial differences in the type of variation with angle of attack exhibited by the two wing-body configurations. At low angles of attack the directional stability of both wing-body configurations appears, as would be expected, to be determined by the body-alone characteristics (fig. 9). It is observed, however, that at the higher angles of attack there are large departures from the body-alone characteristics with the unswept-wing configuration providing a rather rapid reduction in the wing-body instability and the sweptback-wing configuration exhibiting a rather rapid increase in instability in the angle-of-attack range from about 15° to 20° followed by a reduction in instability at the higher angles.

Variations in C_{n_β} of this general type would be expected for wing-alone data about the stability or wind axes since the resultant forces which produce the rolling moments are usually inclined rearward relative to these axes. It would appear unlikely, however, that these thin wings could, at high angles of attack, produce any appreciable yawing moments relative to the body axis about which the present data are presented, since the usual loss of the theoretical leading-edge suction leaves the resultant forces approximately perpendicular to the X body axis. Unfortunately, reliable wing-alone data at high speeds are difficult to obtain; however, the low-speed wing-alone data of reference 3, when transferred to the body axes, appear to substantiate the presumption of a lack of any appreciable isolated wing effect. The large departures from the fuselage-alone directional stability characteristics are most probably associated with wing induced flow over the fuselage afterbody. In an attempt to substantiate this idea, tests were conducted with a large part (13.50 inches) of the fuselage afterbody removed (fig. 2). The lateral-stability derivatives for the unswept- and sweptback-wing—fuselage configurations with the afterbody removed are presented in figure 8. The results indicate that with the fuselage afterbody removed (fig. 8) the large effect of wing sweep on directional stability at high angles of attack shown in figure 7 is eliminated, and the variations of directional stability with angle of attack are similar to those for the fuselage alone (fig. 9). However, C_{l_β} is essentially unaffected by removal of the afterbody; thus, there appears to be no appreciable change in the flow over the wing.

In view of these results, it appears that the large variations of directional stability with angle of attack which exist relative to the body axis for both the unswept- and sweptback-wing—body configurations are due largely to wing (or wing-body) induced sidewash over the fuselage afterbody. The fact that the variations in C_{n_β} are widely different for the two wings is probably associated with differences in the effect of sideslip on the wing spanwise load distribution as reflected in the large differences in the effective dihedral parameter C_{l_β}. In order to illustrate

further the effect of the induced flow over the fuselage afterbody, the differences in the fuselage-alone characteristics have been eliminated by subtracting the appropriate body-alone data (fig. 9) from the wing-body data (figs. 7 and 8); the results are presented in figure 10 for a Mach number of 0.60. In figure 10(b) the results presented for the unswept wing show that above an angle of attack of about 10° rather large values of the increment in directional-stability parameter associated with the wing and mutual interference occur for the configuration having the fuselage afterbody. For the configuration having the fuselage afterbody removed, the increment in directional-stability parameter associated with the wing and mutual interference is essentially zero. In figure 10(a) the corresponding increments for the sweptback-wing—fuselage configurations are presented. The results indicate that removal of a large part of the fuselage rearward of the wing (73 percent of afterbody) considerably reduced the directional instability associated with the sweptback configuration. In addition to the two configurations of the present investigation, the results from a present-day study made in the Langley 7- by 10-foot tunnel are presented. (See fig. 10(a).) This configuration had the cylindrical part of the fuselage extended to the rear of the fuselage; thus, the volume of the afterbody was increased. These results when compared with those of the present investigation indicate that for a given afterbody length a decrease in afterbody volume also results in a sizable improvement in directional stability.

As mentioned previously, these large effects of fuselage afterbody are apparently associated with wing induced sidewash over the fuselage afterbody. In this connection, it is interesting to note that at the higher angles of attack, where the sidewash appears large and of opposite sign for the sweptback and unswept wings (fig. 10), the rolling moment due to sideslip is considerably different for the two wings. (See fig. 7.) These differences in rolling moments indicate differences in span loadings which could produce sidewash of opposite sign for the two wings.

Several inconsistencies appear to exist for the sweptback wing. For example, although the yawing moment induced on the fuselage afterbody occurs above an angle of attack of about 12° (fig. 10), the largest variations of C_{l_β} occur below this angle. (See fig. 7.) In addition, it is observed that while zero C_{l_β} occurs at an angle of attack of 22° (fig. 7(a)) a large yawing moment associated with the fuselage afterbody occurs at this angle of attack. (See fig. 10.)

A possible explanation lies in the argument, presented in reference 7, that, except for possible effects of sideslip on the induced angle, the local circulation will be unaffected by sideslip and will remain symmetrical despite an unsymmetrical spanwise distribution of lift. Stated slightly differently from that in reference 7 the argument is as follows: If the simple-sweep theory is applied to a wing in sideslip by means of lifting-line theory (ref. 8), the velocity normal to the quarter-chord line of the

retreating wing panel is altered by the factor $\frac{\cos(\Lambda + \beta)}{\cos \Lambda}$ and the angle of attack with respect to this velocity is altered by the reciprocal of the same factor. The lift is proportional to the angle of attack and the velocity squared and is therefore affected by sideslip. However, since the circulation is proportional to the angle of attack and the first power of the velocity, the sideslip effects are compensating, and it appears that no change in circulation occurs with potential flow. In addition, the nonpotential effects that occur at moderate and high angles of attack represent changes in circulation which, in view of the effect on C_{l_β}, are probably not symmetrical across the span. Under these conditions, it is conceivable that the asymmetrical circulation can combine in such a manner with the asymmetrical distribution of the velocity normal to the quarter-chord line as to produce little rolling moment on the wing but large sidewash velocities in the flow field behind the wing. This phenomenon could account for the previously mentioned examples, with regard to the sweptback-wing—fuselage combination, where zero total C_{l_β} was accompanied by a large yawing moment induced on the fuselage afterbody and where changes in sign of C_{l_β} were not accompanied by changes in the induced yawing moment.

An indication of the effect of Mach number at subsonic speeds on the contribution of the wing and the fuselage afterbody to directional stability is presented in figure 11 for the sweptback-wing configuration. The present investigation was made at Mach numbers of 0.60 and 0.80; and the results, presented in figure 11(a), indicate a reduction in the directional instability contributed by interference on the fuselage afterbody with increasing Mach number. In order to substantiate further this trend with Mach number, the results from reference 9 (converted to body axis) obtained with a similar configuration for a larger Mach number range are presented in figure 11(b). Results for Mach numbers from 0.40 to 0.91 are presented and the reduction in the directional instability with increasing Mach number is evident. This reduction is apparently due, in part, to a decrease in the wing circulation asymmetry that is implied by the effect of Mach number on C_{l_β}. (See fig. 7 and ref. 9.) In regard to the fact that value of $\Delta C_{n_{\beta(WF-F)}}$ is considerably less for the configuration of reference 9 at corresponding Mach numbers, it should be noted that, in addition to the difference in wing taper ratios, the fuselage afterbody is somewhat shorter than that of the configuration presented in figure 11(b).

CONCLUDING REMARKS

A study of subsonic wind-tunnel tests showed that large variations in the directional stability characteristics of wing-fuselage combinations can occur in moderate and high angle-of-attack ranges easily encountered in spins and rolling maneuvers. For unswept-wing—fuselage combinations positive directional stability can occur at high angles of attack, whereas for sweptback-wing—fuselage combinations an increase in the usual instability occurs at high angles of attack. The results obtained for both configurations apparently are caused by wing induced sidewash on the fuselage afterbody.

Langley Aeronautical Laboratory,
National Advisory Committee for Aeronautics,
Langley Field, Va., September 12, 1956.

REFERENCES

1. Stone, Ralph W., Jr., and Klinar, Walter J.: The Influence of Very Heavy Fuselage Mass Loadings and Long Nose Lengths Upon Oscillations in the Spin. NACA TN 1510, 1948.

2. Phillips, William H.: Effect of Steady Rolling on Longitudinal and Directional Stability. NACA TN 1627, 1948.

3. Letko, William, and Williams, James L.: Experimental Investigation at Low Speed of Effects of Fuselage Cross Section on Static Longitudinal and Lateral Stability Characteristics of Models Having 0° and 45° Sweptback Surfaces. NACA TN 3551, 1955.

4. Herriot, John G.: Blockage Corrections for Three-Dimensional-Flow Closed-Throat Wind Tunnels, With Consideration of the Effect of Compressibility. NACA Rep. 995, 1950. (Supersedes NACA RM A7B28.)

5. Gillis, Clarence L., Polhamus, Edward C., and Gray, Joseph L., Jr.: Charts for Determining Jet-Boundary Corrections for Complete Models in 7- by 10-Foot Closed Rectangular Wind Tunnels. NACA WR L-123, 1945. (Formerly NACA ARR L5G31.)

6. Polhamus, Edward C.: Jet-Boundary-Induced-Upwash Velocities for Swept Reflection-Plane Models Mounted Vertically in 7- by 10-Foot, Closed, Rectangular Wind Tunnels. NACA TN 1752, 1948.

7. Queijo, M. J.: Theoretical Span Load Distributions and Rolling Moments for Sideslipping Wings of Arbitrary Plan Form in Incompressible Flow. NACA Rep. 1269, 1956. (Supersedes NACA TN 3605.)

8. Toll, Thomas A., and Queijo, M. J.: Approximate Relations and Charts for Low-Speed Stability Derivatives of Swept Wings. NACA TN 1581, 1948.

9. Wiggins, James W., Kuhn, Richard E., and Fournier, Paul G.: Wind-Tunnel Investigation To Determine the Horizontal- and Vertical-Tail Contributions to the Static Lateral Stability Characteristics of a Complete-Model Swept-Wing Configuration at High Subsonic Speeds. NACA TN 3818, 1956. (Supersedes NACA RM L53E19.)

TABLE I
FUSELAGE ORDINATES

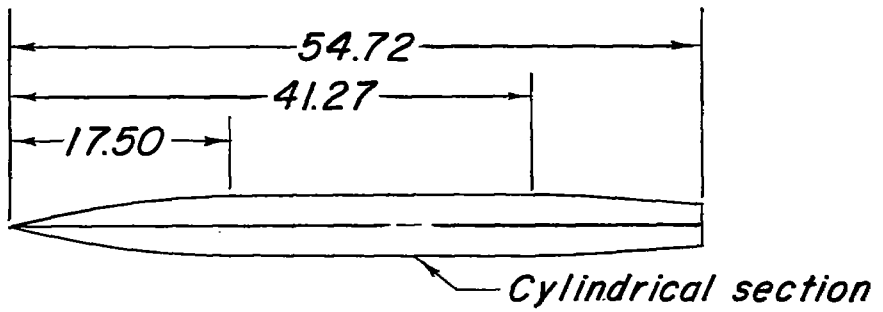

Ordinates

Station, in.	Radius, in.
0	0
2.00	.53
4.00	1.00
6.00	1.44
8.00	1.80
10.00	2.07
12.00	2.30
14.00	2.42
16.00	2.47
17.50	2.50
41.27	2.50
43.27	2.42
45.27	2.35
47.27	2.25
48.30	2.14
54.72	1.65

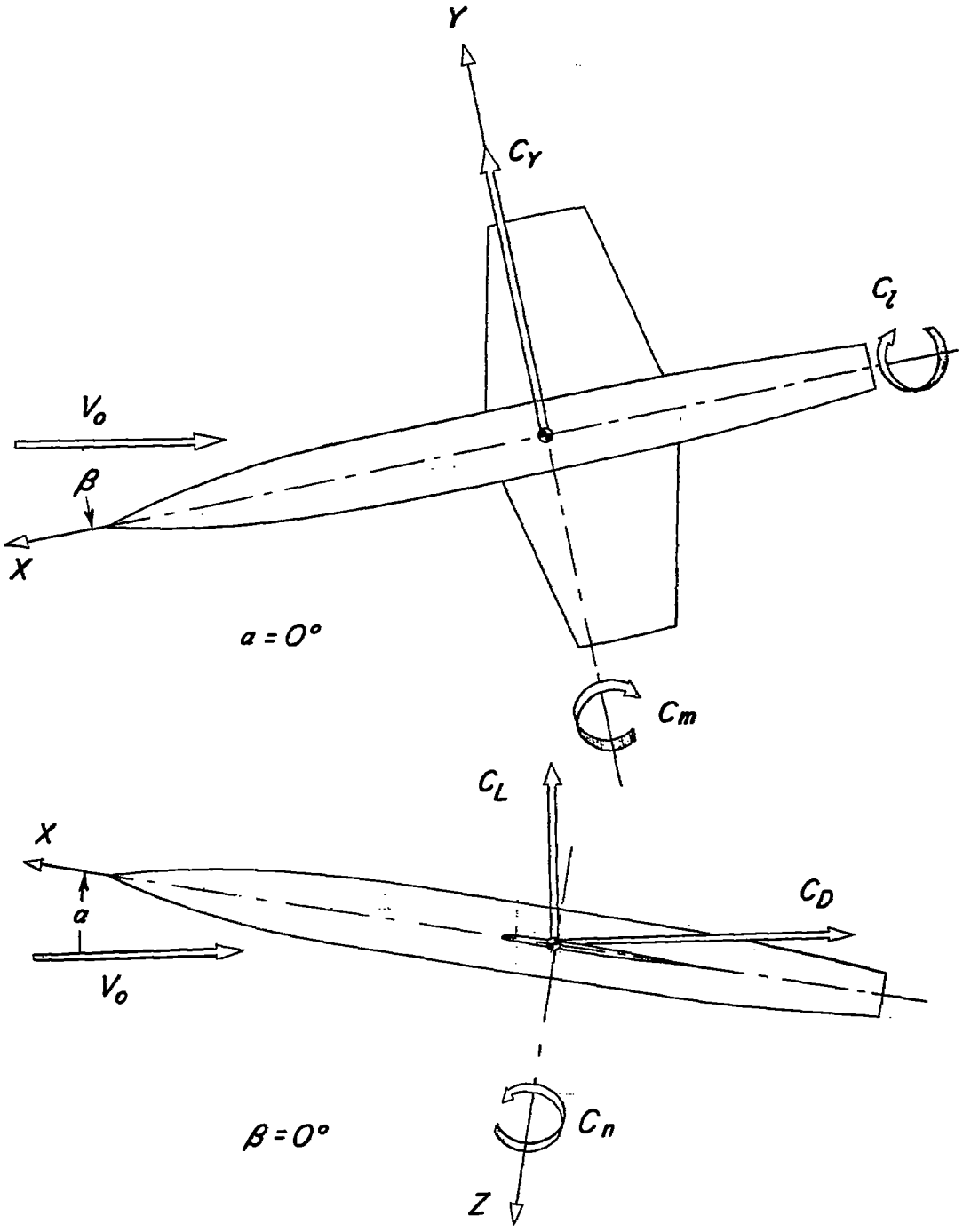

Figure 1.- Convention used to define positive sense of forces, moments, and angles.

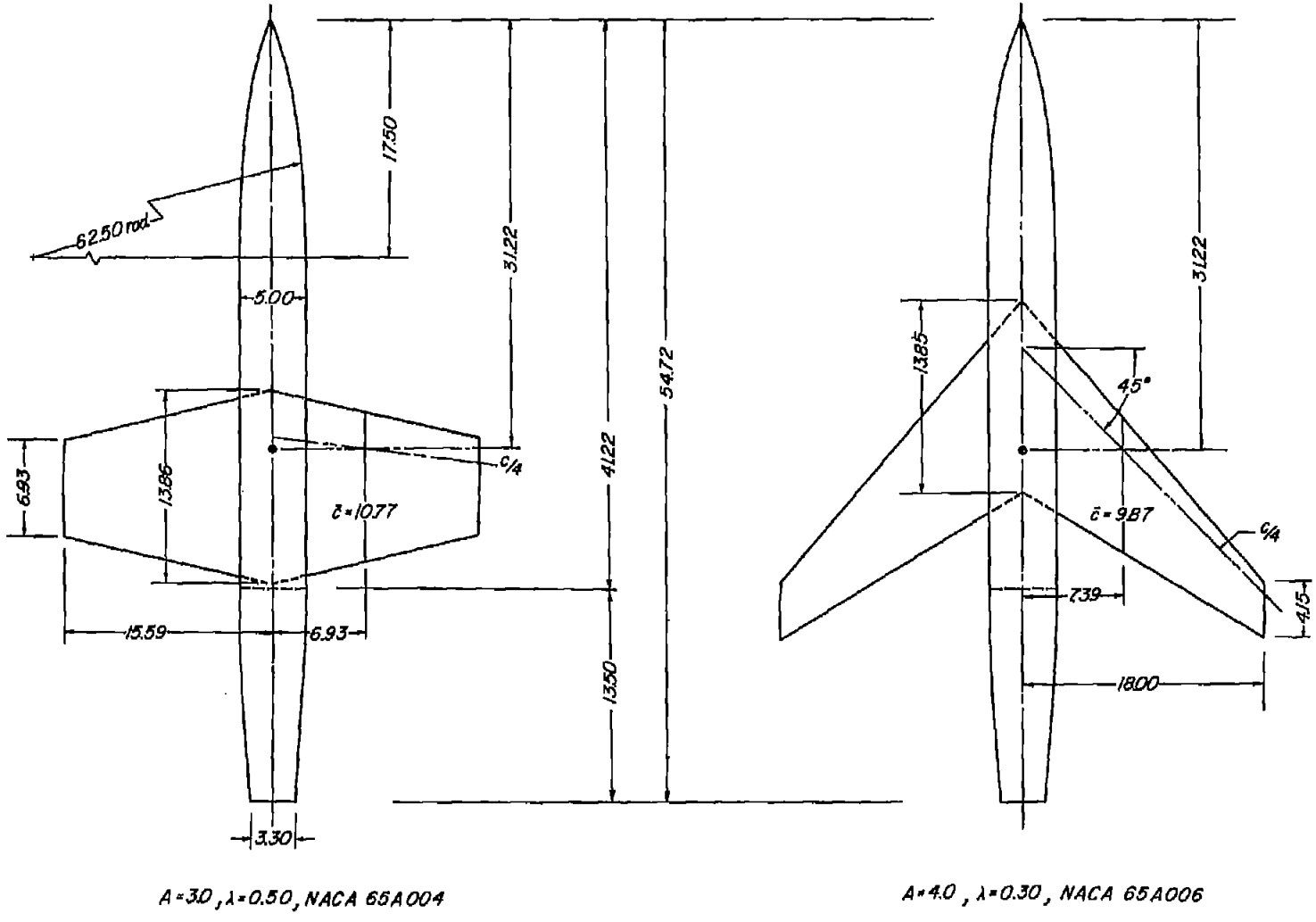

Figure 2.- Drawings of models employed. (All dimensions are in inches.)

L-93867

Figure 3.- Model installed in Langley high-speed 7- by 10-foot tunnel.

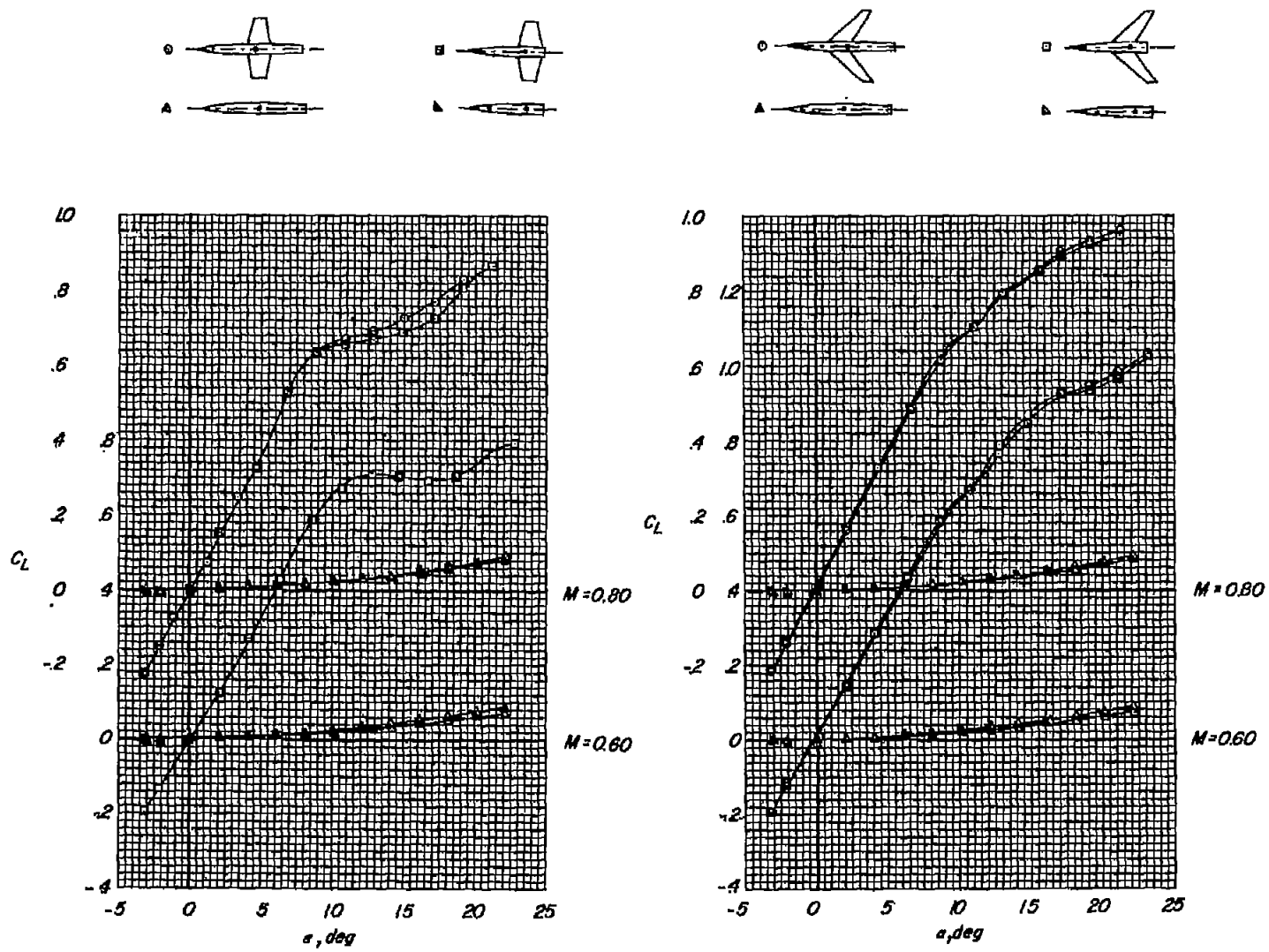

Figure 4.- Variation of lift characteristics with angle of attack for models employed.

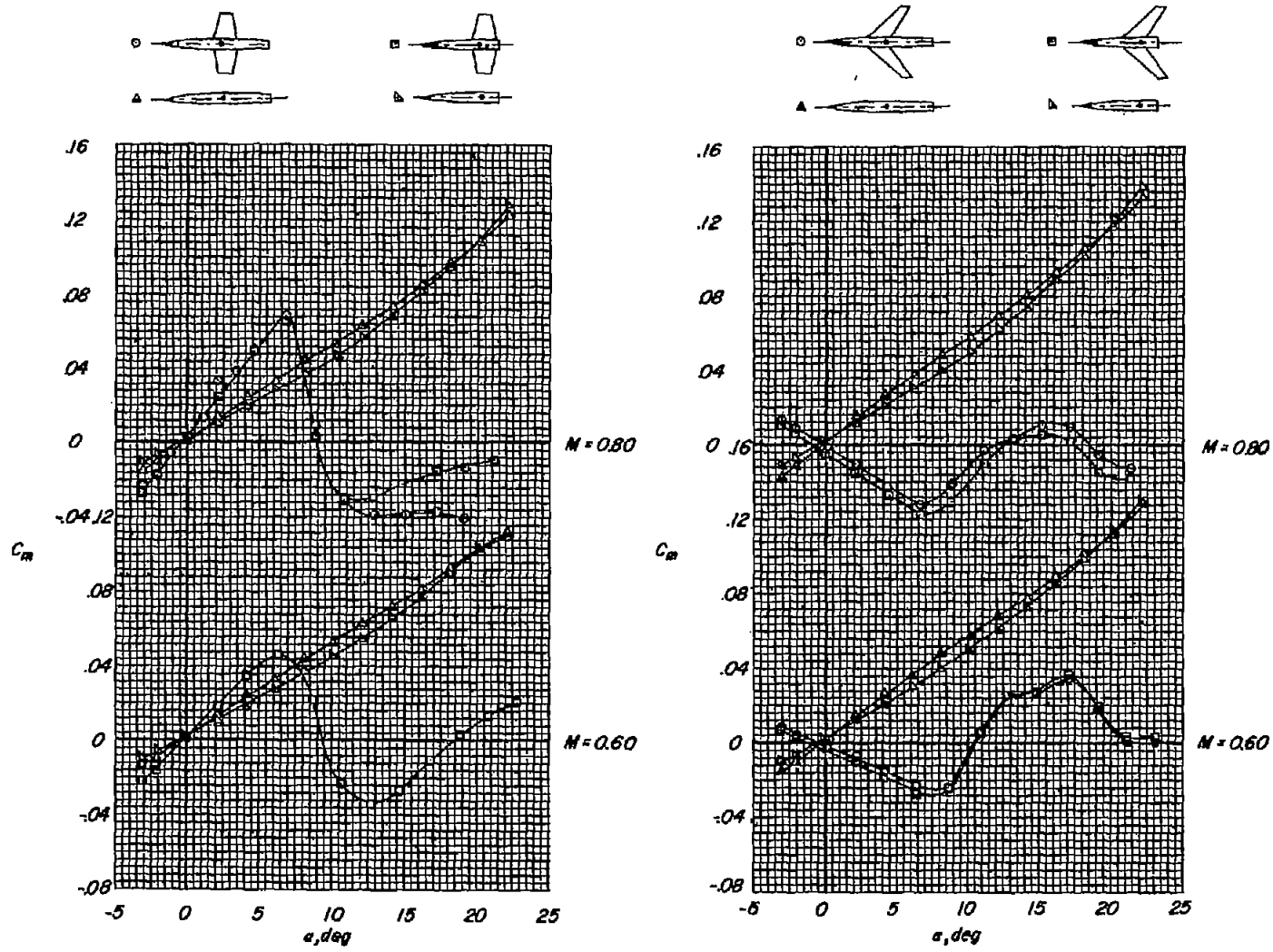

Figure 5.- Variation of pitching-moment characteristics with angle of attack for models employed.

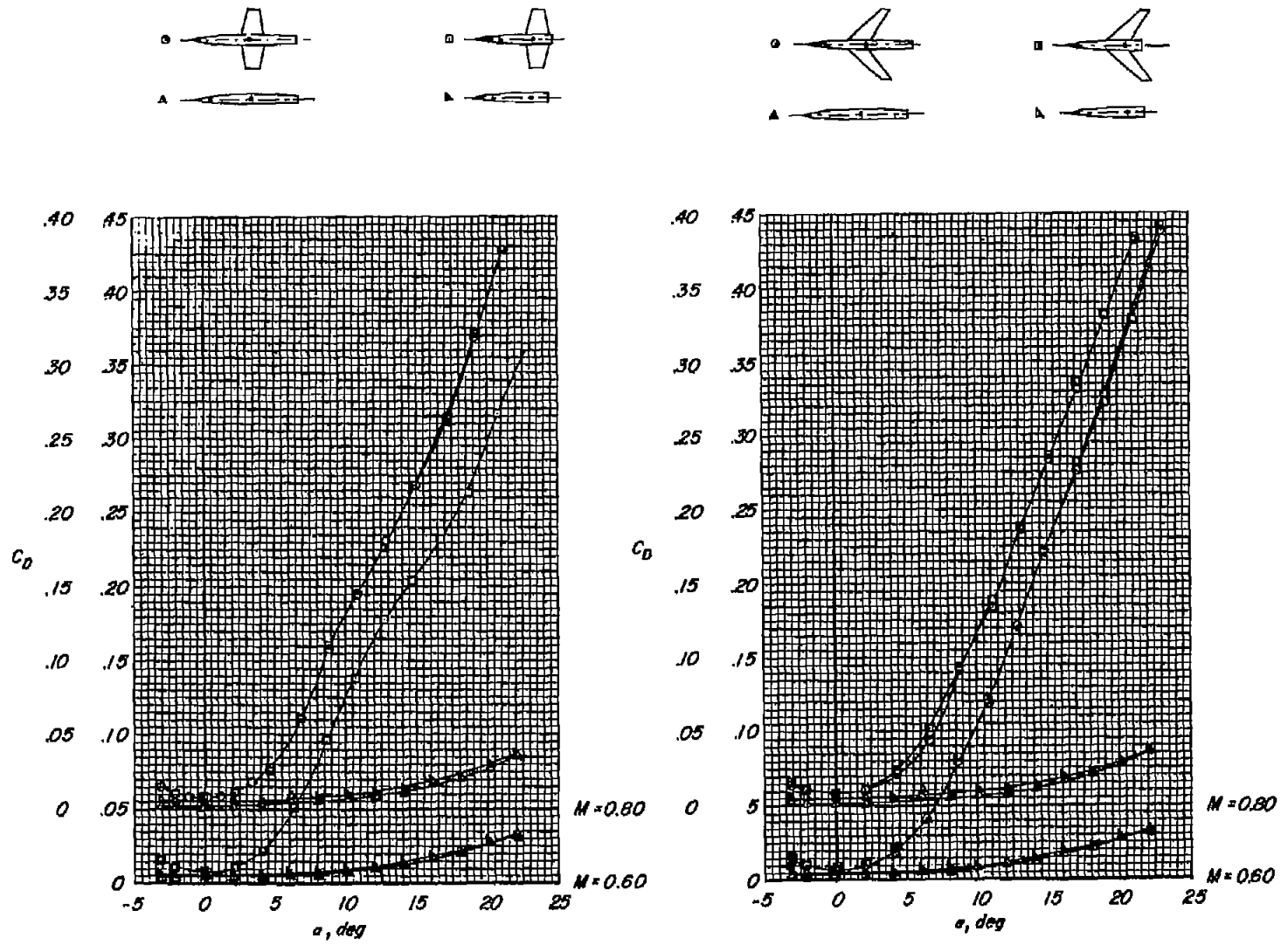

Figure 6.- Variation of drag characteristics with angle of attack for models employed.

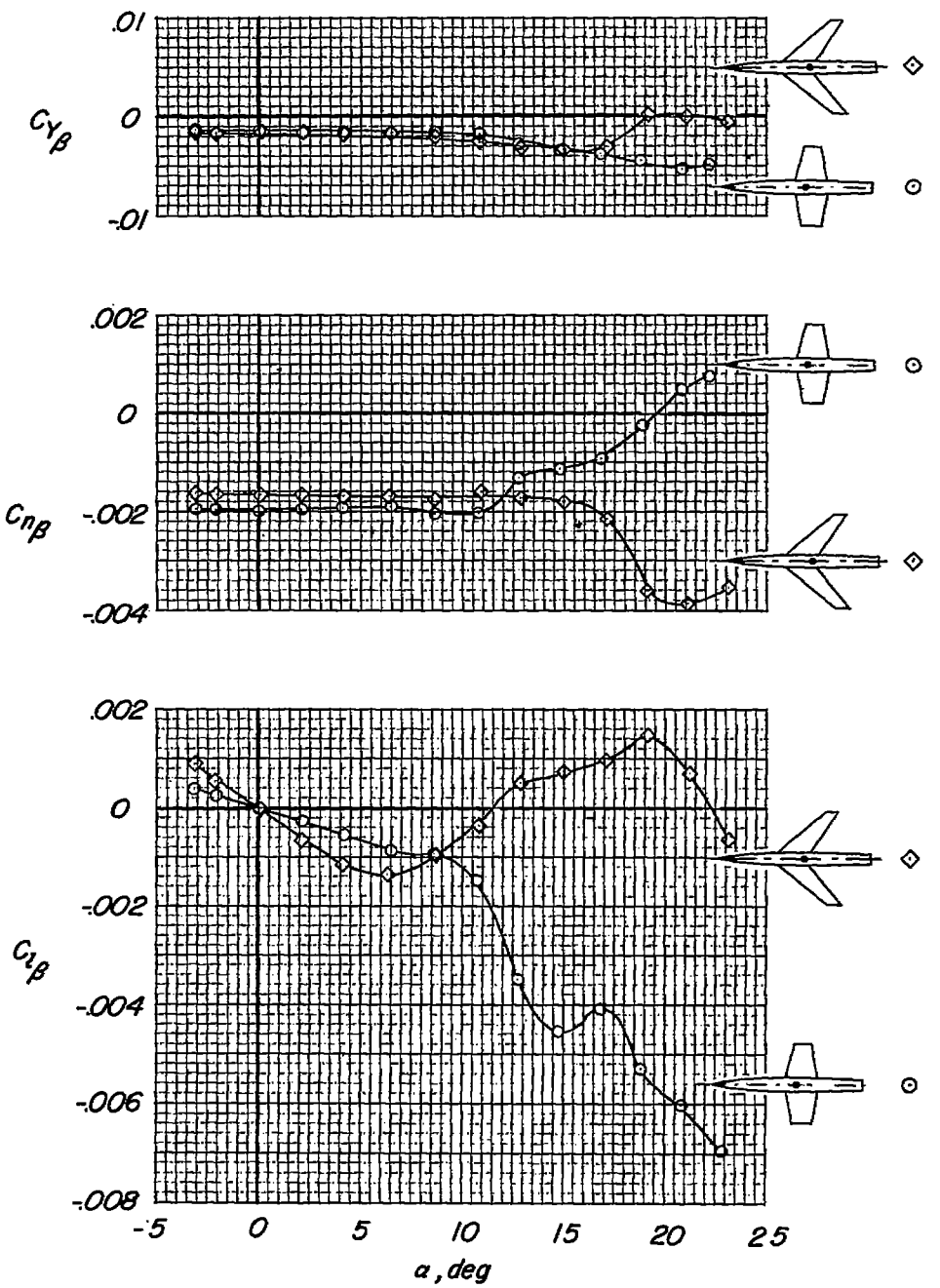

(a) M = 0.6.

Figure 7.- Variation of lateral-stability parameters with angle of attack for models with fuselage afterbody.

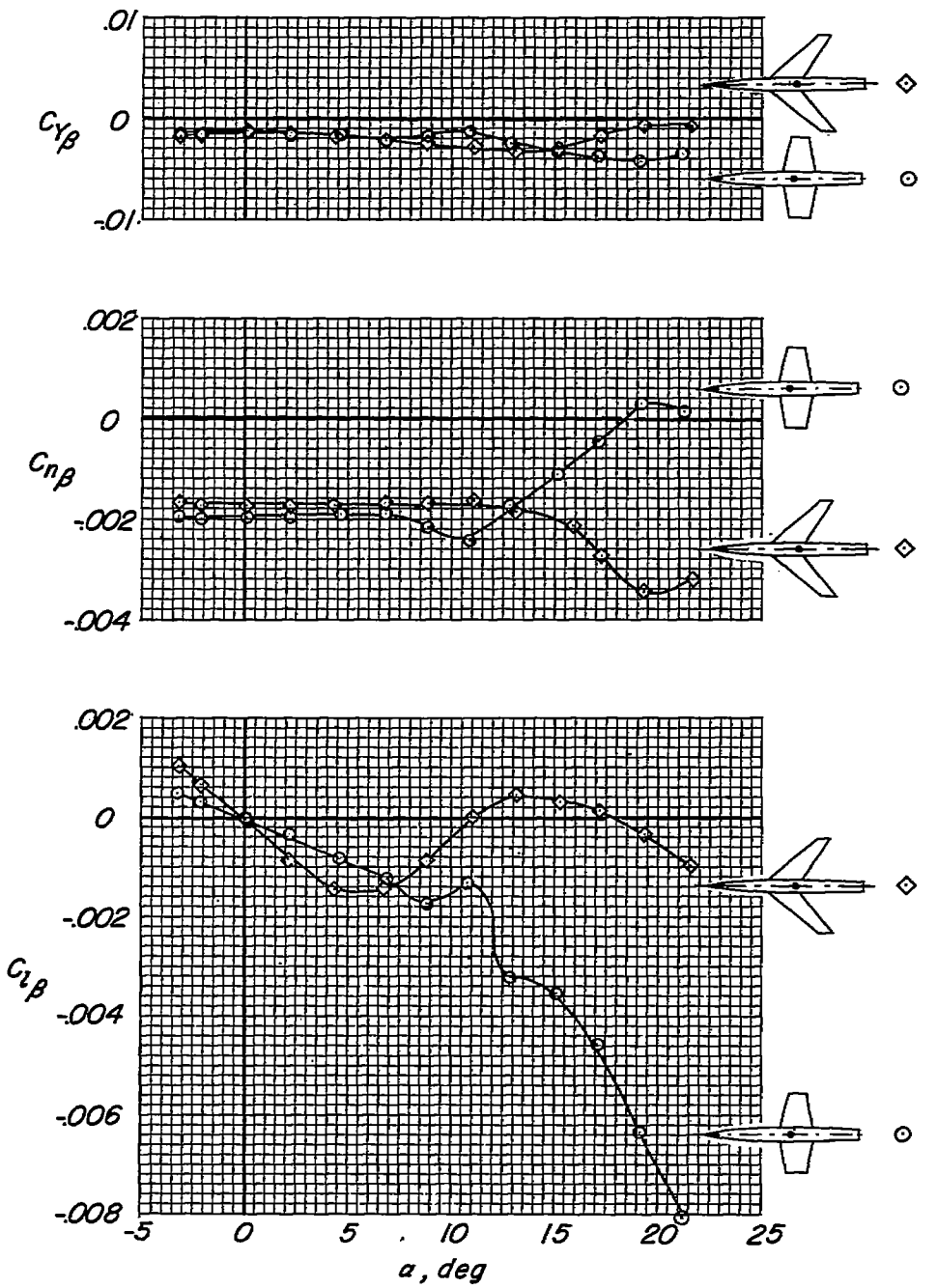

(b) M = 0.8.

Figure 7.- Concluded.

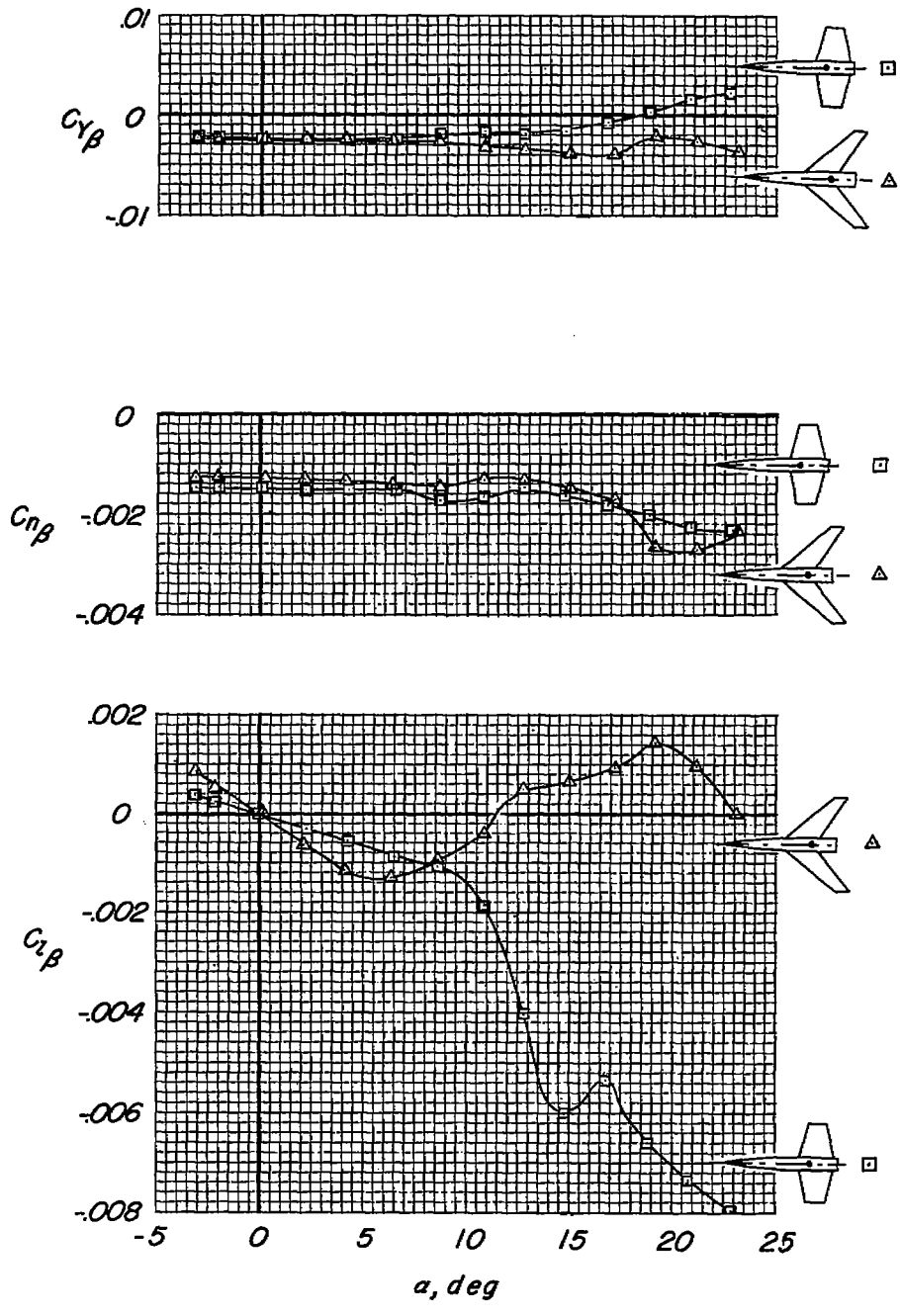

(a) M = 0.6.

Figure 8.- Variation of lateral-stability parameters with angle of attack for models with fuselage afterbody removed.

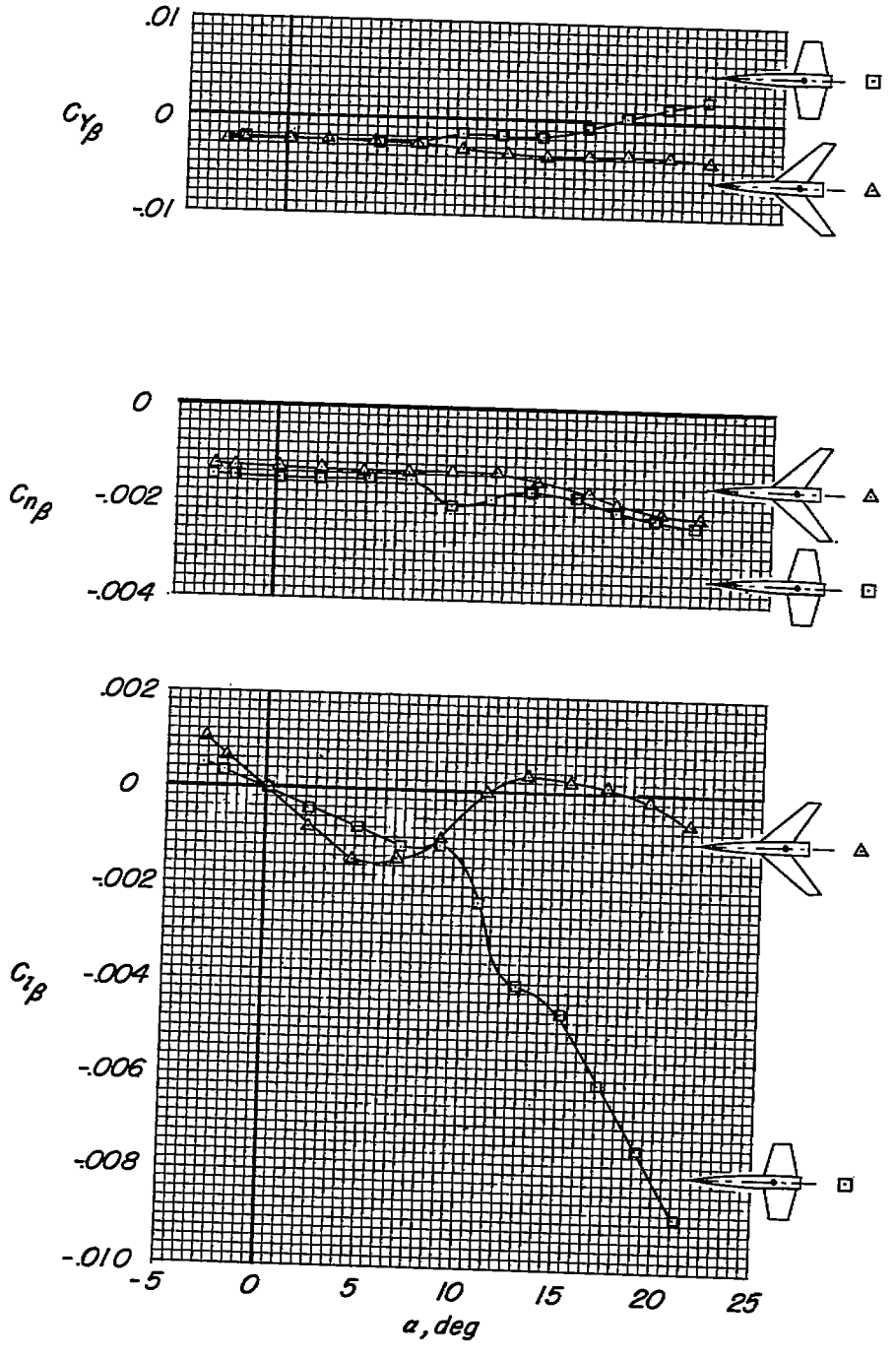

(b) M = 0.8.

Figure 8.- Concluded.

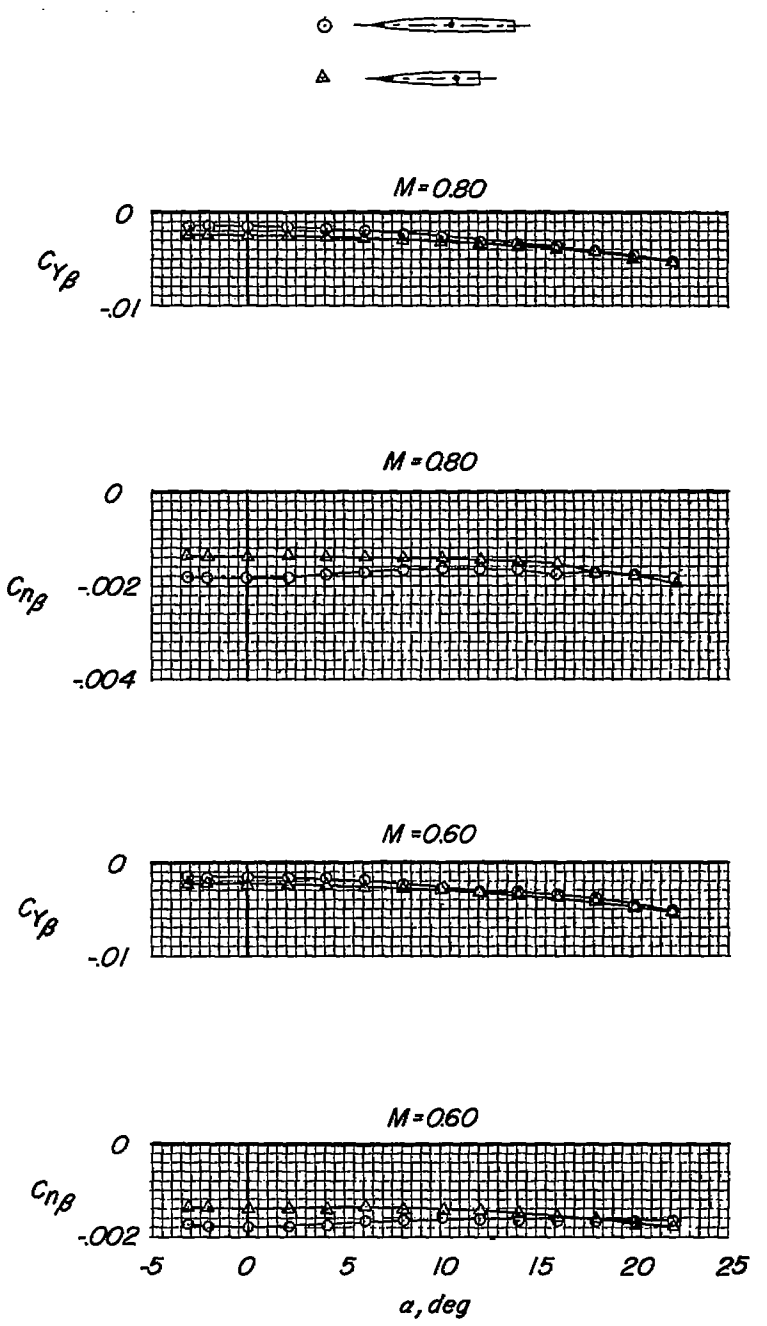

(a) Based on sweptback wing.

Figure 9.- Variation of lateral-stability parameters with angle of attack for fuselage alone with and without afterbody.

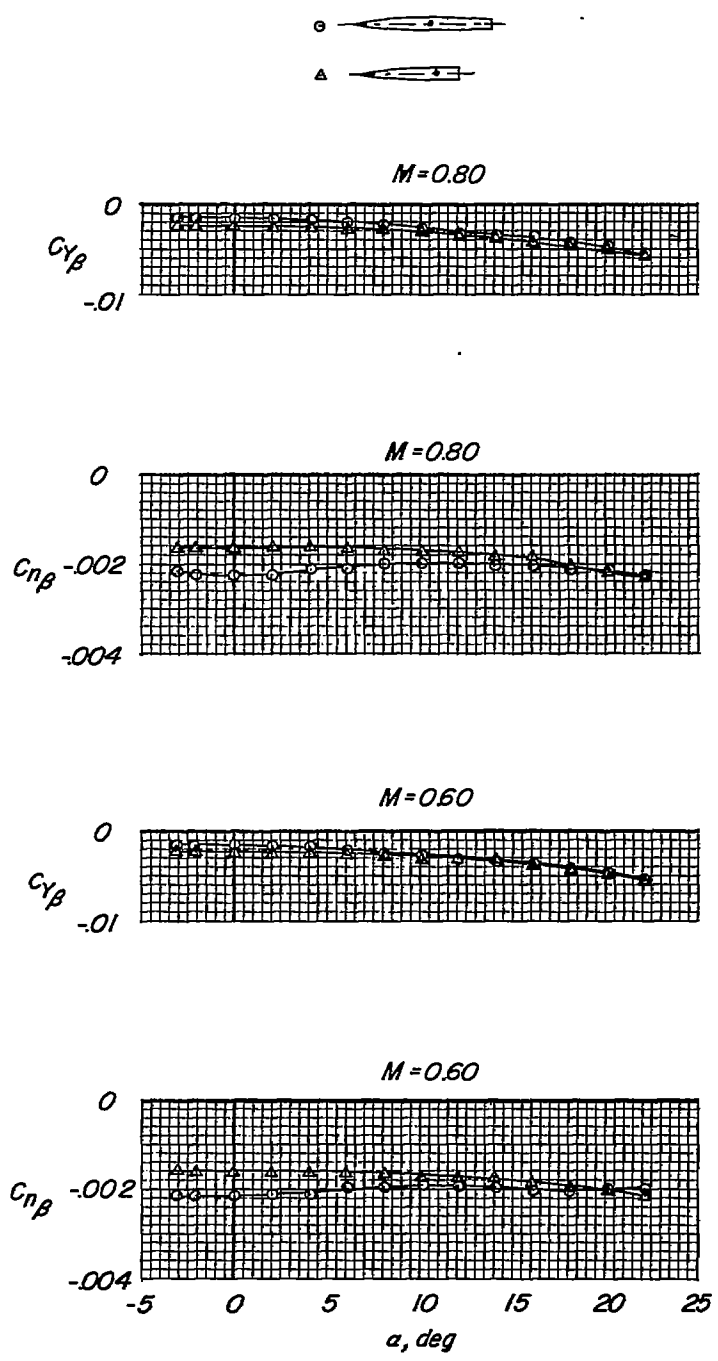

(b) Based on unswept wing.

Figure 9.- Concluded.

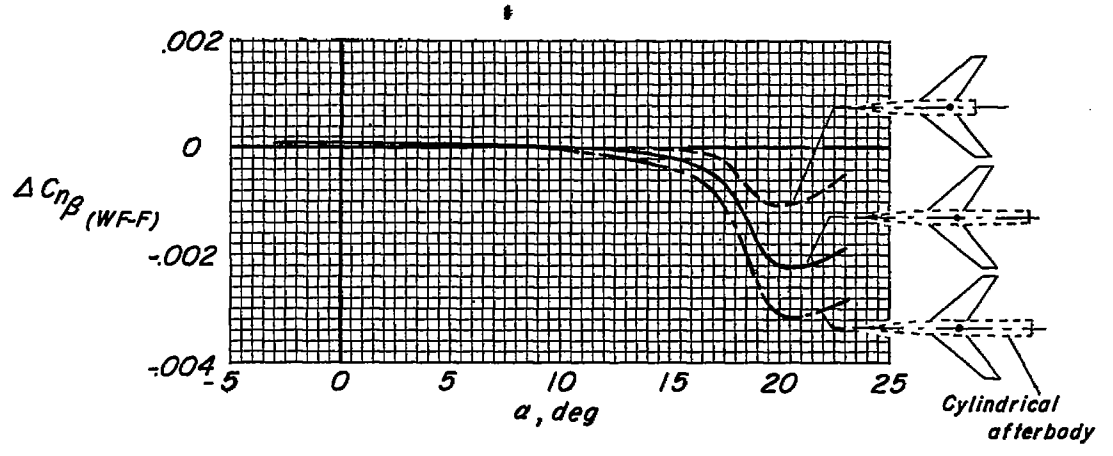

(a) Sweptback wing.

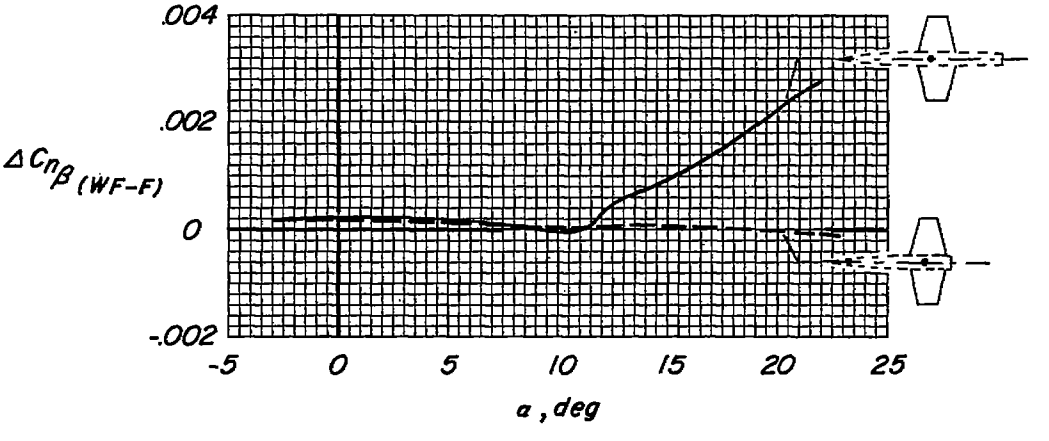

(b) Unswept wing.

Figure 10.- Effect of fuselage afterbody on the directional stability contributed by wing and mutual interference; M = 0.60.

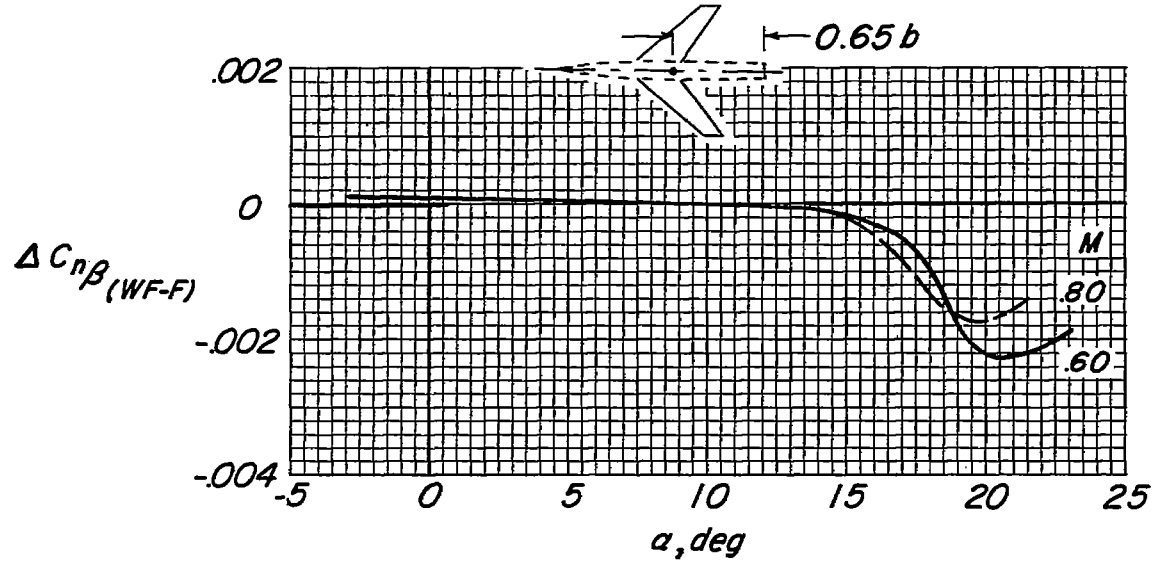

(a) Present tests; $\lambda = 0.30$.

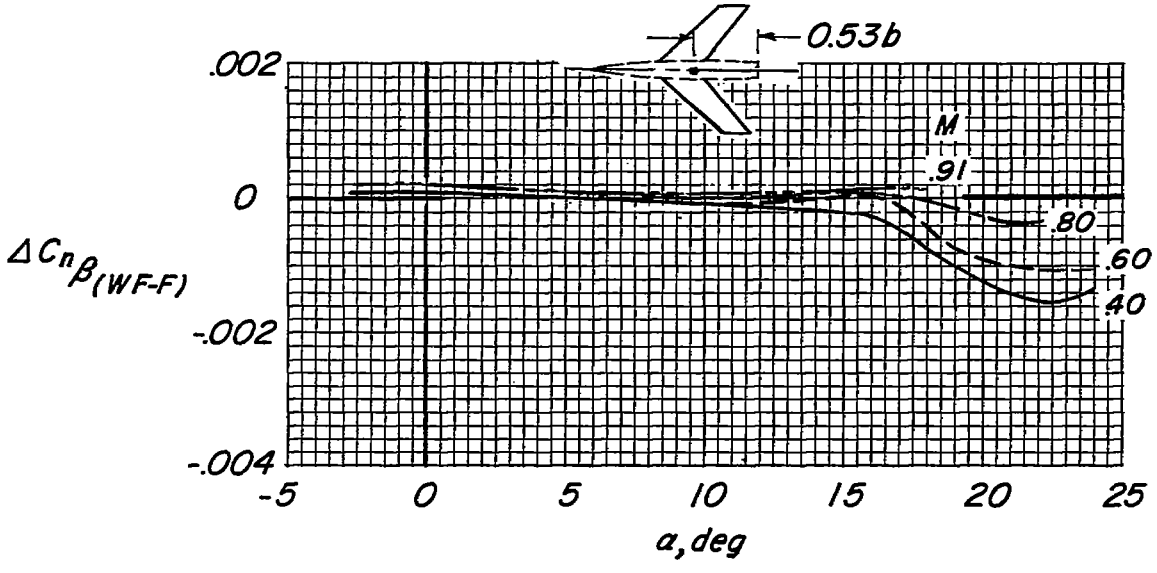

(b) From reference 9; $\lambda = 0.60$.

Figure 11.- Effect of Mach number on directional stability contributed by wing and mutual interference (body axes); $\lambda = 45^\circ$, A = 4, NACA 65A006 airfoil.